



Search for a Standard Model Higgs Boson Decaying Into Photons at CDF Using 10 fb^{-1} of Data

The CDF Collaboration
URL <http://www-cdf.fnal.gov>
(Dated: July 26, 2012)

A search for the SM Higgs boson in the diphoton mass spectrum is reported using data corresponding to an integrated luminosity of up to 10 fb^{-1} . We improve upon the previous CDF result by increasing the amount of data included by 43%. No excess is observed in the data over the background prediction and 95% C.L. upper limits are set on the production cross section times the $H \rightarrow \gamma\gamma$ branching fraction for hypothetical Higgs boson masses between 100 and 150 GeV/c^2 .

Preliminary Results

I. INTRODUCTION

Low mass standard model (SM) Higgs boson searches at the Tevatron usually focus on the dominant $b\bar{b}$ decay channel. The branching fraction for the diphoton ($\gamma\gamma$) final state $B(H \rightarrow \gamma\gamma)$ is very small, with a maximal value of approximately 0.23% for a Higgs boson mass of $125 \text{ GeV}/c^2$. The diphoton final state is appealing, however, due to its cleaner signature compared to b jets. The better reconstruction efficiency for photons provides a larger relative acceptance of $H \rightarrow \gamma\gamma$ events and the photon's better energy resolution leads to a narrow mass peak, which is a powerful discriminant against smoothly falling diphoton backgrounds. These experimental features help make the diphoton final state one of the most promising search modes for Higgs boson masses below $140 \text{ GeV}/c^2$ for ATLAS and CMS experiments at the LHC. Most recently, the ATLAS (CMS) $H \rightarrow \gamma\gamma$ search reports preliminary findings of an excess of events above the expected background at $m_H = 126.5 \text{ GeV}/c^2$ ($125 \text{ GeV}/c^2$), with a local significance of 4.5σ (4.1σ) [1, 2]. The signal sensitivity at the Tevatron is smaller (see Ref. [3] and [4] for recent results) however, we pursue this channel still, not only because it is interesting to make a statement on the sensitivity of CDF to the SM $H \rightarrow \gamma\gamma$ process, but also in order to contribute sensitivity to CDF's combined Higgs boson searches along with the overall Tevatron Higgs search.

In addition to SM $H \rightarrow \gamma\gamma$ production, one can devise many possible Beyond the Standard Model (BSM) scenarios where $B(H \rightarrow \gamma\gamma)$ is enhanced. An informative summary of the various models that modify $B(H \rightarrow \gamma\gamma)$ can be found in Reference [5]. Any resonance observed could also then be evidence for a BSM Higgs.

Here, we present a search of the diphoton mass spectrum for signs of a resonance and interpret results in the context of a SM scenario. Reference [6] describes an interpretation of the results for a fermiophobic Higgs boson model. We update the most recent 7.0 fb^{-1} analysis in this channel [4] with the incorporation of the final diphoton dataset taken up to the Tevatron shutdown in September, 2011.

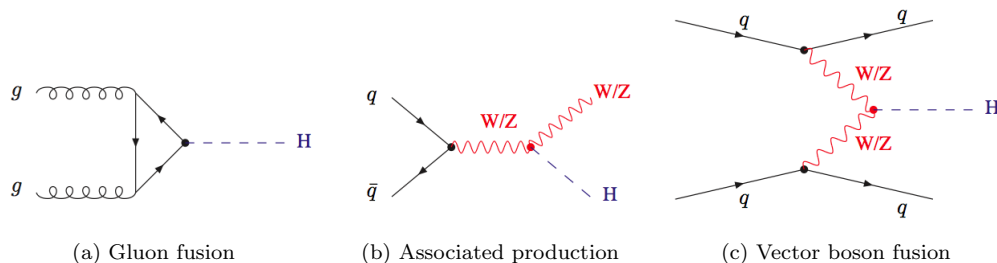


FIG. 1: The dominant production mechanisms at the Tevatron for the SM Higgs boson.

The three most dominant production mechanisms at the Tevatron are considered: gluon fusion (GF), associated production where the Higgs boson is produced with a W or Z boson (VH), and vector boson fusion (VBF). Production diagrams for all three processes are shown in Fig. 1, where the corresponding cross sections are given in Table I. Branching fractions are calculated by HDECAY [7] and are also given in Table I.

Diphoton events are divided into four independent subsamples according to the position and type of the photon candidate. In CC events (the most sensitive category), there are two photons in the central region of the detector. In CP events, one photon is in the central region and one is the plug region. For each of these categories, the two highest p_T photons in the sample are selected. If a CC or CP event is not identified, then two additional categories are considered. In $C'C$ events, both photons are central but one has converted and is reconstructed from its e^+e^- decay products. Finally, in $C'P$ events, one photon is in the plug region and the other is a central conversion photon.

II. THE CDF DETECTOR

The CDF detector is described in many available references [8, 9].

III. DATA SETS AND GLOBAL EVENT SELECTION

This analysis uses data from February 2004 through September 2011, comprising 10.0 fb^{-1} of integrated luminosity for the CC category, and 9.34 , 9.87 , and 9.28 fb^{-1} for the CP, $C'C$, and $C'P$ categories, respectively. Signal Monte

m_H (GeV/ c^2)	σ_{GF} (fb)	σ_{WH} (fb)	σ_{ZH} (fb)	σ_{VBF} (fb)	$B(H \rightarrow \gamma\gamma)$ (%)
100	1821.8	281.1	162.7	97.3	0.159
105	1584.7	238.7	139.5	89.8	0.178
110	1385.0	203.7	120.2	82.8	0.197
115	1215.9	174.5	103.9	76.5	0.213
120	1072.3	150.1	90.2	70.7	0.225
125	949.3	129.5	78.5	65.3	0.230
130	842.9	112.0	68.5	60.5	0.226
135	750.8	97.2	60.0	56.0	0.214
140	670.6	84.6	52.7	51.9	0.194
145	600.6	73.7	46.3	48.0	0.168
150	539.1	64.4	40.8	44.5	0.137

TABLE I: Cross sections for SM Higgs production for gluon fusion (GF), associated production with a W or Z boson (WH and ZH respectively), and vector boson fusion (VBF). The last column provides branching ratios for SM $H \rightarrow \gamma\gamma$ decays, in percent.

Carlo (MC) was generated using PYTHIA 6.2 [10], CTEQ5 [11] parton distribution functions, and the standard CDF underlying event tune [12]. Samples for masses between 100 – 150 GeV/ c^2 in 5 GeV/ c^2 intervals were developed and used.

The events are selected by a three-level trigger system that requires an isolated cluster of energy deposited in the EM calorimeter with a transverse energy $E_T > 25$ GeV [25]. The trigger efficiency for events that pass the full diphoton selection is essentially 100% for the most sensitive event category (CC) and above 90% for all other categories. The global event selection then requires that the data included in the analysis was taken during good detector conditions. The reconstructed event vertex is determined from the vertex with highest sum p_T of the associated tracks, and the z position of this vertex must be within 60 cm of zero. The overall efficiency for this cut, measured from the data, is $97.43 \pm 0.07\%$.

IV. PHOTON IDENTIFICATION

The dominant backgrounds to prompt photons originating from the event vertex are electrons faking photons and jets faking photons. The latter is more frequent and typically occurs when a jet fragments into a π^0 or η meson which then decays to multiple photons. These delayed photons are collinear and are often mis-reconstructed as a single photon. A set of photon selection requirements are then applied in order to identify high-energy prompt photons with $p_T > 15$ GeV/ c , and to reduce these backgrounds.

A. Central Photon ID

A neural network (NN) technique is used to identify photons in the central region of the detector ($|\eta| < 1.05$). Central photon candidates are first required to satisfy loose selection requirements as described in Ref. [13]. After additional track requirements are applied to remove electrons, the remaining candidates are required to have a NN output value above a threshold that is selected to maximize a $H \rightarrow \gamma\gamma$ signal to background figure of merit. As more than half of the events in the data with two photon candidates contain either one or two jets misidentified as a prompt photon, the NN discriminant is trained using photon and jet MC samples and constructed from several detector variables that distinguish true photons from these jet backgrounds. These variables also allow the NN method to be applied to electrons, which are used to calibrate ID efficiencies. These variables include the ratio of energy in the shower maximum detector to that in the calorimeter cluster associated with the photon, the ratio of hadronic to EM transverse energy (Had/EM), calorimeter and track isolation [13], and a χ^2 value calculated by comparing the measured transverse shower profile to that of a single EM shower [14].

This NN method increases the photon signal efficiency by $\sim 5\%$ and background rejection by $\sim 12\%$ compared to the standard selection requirements for central photons [13], which improves $H \rightarrow \gamma\gamma$ sensitivity by about 9%. Signal efficiency is calculated using $Z \rightarrow e^+e^-$ events in both the data and MC, as a function of the number of vertices (N_{vtx}) in the event. Net efficiencies for the data and simulation are obtained by taking the weighted average of the efficiencies over the number of vertices in the diphoton sample and Higgs signal MC. A data-MC scale factor is then determined based on the difference in the signal efficiency as measured from the data relative to that predicted by the MC. This correction factor is included when normalizing the Higgs signal mass shape.

Several sources of systematic uncertainty were considered. Photon ID efficiencies are studied using electrons from Z boson decays; however, there are small differences in the shower profiles of electrons and photons which may affect these studies. To account for this, a systematic of 1% was taken based on the difference between photon and electron ID efficiencies observed in the MC with detector simulation. For this comparison, $\gamma \rightarrow e^+e^-$ conversions were removed from the photon MC which are not in the Z MC. An uncertainty of 0.2% on the efficiency of removing these conversions is applied and is due to the uncertainty in the material included in the simulation of the CDF detector. A single data-MC scale factor is applied to the full MC sample; however, the variations of this factor between data taking periods was included as a systematic of 1.5%. Finally, the uncertainties on the Z boson mass fits in data and MC used to study ID efficiencies are propagated as an uncertainty of 0.2%.

B. Plug Photon ID

We include photons with $1.2 < |\eta| < 2.8$ using standard CDF photon ID [13] based on similar variables described for central photons: the ratio of energy in the shower maximum detector to that in the calorimeter cluster associated with the photon, the ratio of hadronic to EM transverse energy (Had/EM), calorimeter and track isolation [13], and a χ^2 value calculated by comparing the measured transverse shower profile to that of a single EM shower [14]. Data-MC scale factors are obtained and applied to the normalization of the Higgs signal mass shape using the same techniques as for central photons. The same sources of systematic uncertainty on photon ID for central photons are applied to plug photons. Uncertainty from the difference between electron vs photon ID is taken to be 2.6%, from detector material to be 3.0%, from data taking periods to be 2.0%, and from data/MC fits of the Z mass to be 0.8%.

C. Central Conversion Photon ID

As photons pass through detector material, electromagnetic interactions with a nucleus can cause photons to convert into an electron-positron pair. Using photon MC truth information it was found that this occurs approximately 15% of the time in the central region of the detector, so for the CC channel about 26% of events are lost (where we ignore double conversion events). Due to lower tracking efficiency in the plug region we only consider central conversion photons.

In order to recover central conversion photons, we search for an electron with $|\eta| < 1.05$ (the “primary” and higher E_T leg) with a nearby track corresponding to a particle of opposite charge and with a minimum $p_T = 1.0$ GeV/c (the “secondary” leg). The proximity of the two particle tracks is first determined by requiring the transverse distance between the two tracks to be less than 0.2 cm at the radial location where they are parallel. The difference in $\cot \theta$ between the two tracks must be less than 0.04, where $\cot \theta = p_z/p_T$. Backgrounds are further removed by allowing only a small fraction of hadronic E_T associated with the primary electron’s cluster. Additionally, requirements are made on the conversion candidate’s calorimeter isolation. This quantity is obtained from the primary electron’s calorimeter isolation [13], with the secondary electron’s p_T subtracted if its track points to a different calorimeter ϕ tower. The ratio of transverse energy to transverse momentum (E/p) shape is peaked at one for isolated photon conversions, but has a long tail for photon conversions from π^0 or $\eta \rightarrow \gamma\gamma$ decays due to the extra energy from the unconverted photon. Restrictions on this ratio then further remove jet backgrounds. The conversion E_T is obtained from the primary electron’s E_T with the secondary electron’s p_T added if it is in a different calorimeter tower while the photon’s reconstructed transverse momentum is obtained by adding the vector sum of the two track’s momenta at the radius of the conversion.

The direction of the conversion photon’s momentum is obtained by taking the vector sum of the individual track momenta; however, better $H \rightarrow \gamma\gamma$ mass resolution is obtained by setting the total momentum to be the conversion’s energy obtained from EM calorimeters, which additionally constrains the photon’s mass to zero.

An uncertainty on this selection is obtained using $Z \rightarrow e^\pm +$ trident events in the data and MC, where a trident is defined as an electron that radiates a photon via bremsstrahlung which then converts to an electron-positron pair ($e^\mp\gamma \rightarrow e^\mp e^+e^-$). Due to the lower energy range of the conversion photons of this method compared to those from $H \rightarrow \gamma\gamma$, it was chosen not to apply a data-MC scale factor to simulated events but instead to use the difference in the calculated scale factor from one to obtain an uncertainty on conversion ID. This was estimated by comparing the ratio of number of trident events selected to the number of regular $Z \rightarrow e^+e^-$ events selected in both the data and MC. This ratio was chosen in order to remove dependence on uncertainties from sources such as trigger efficiency, luminosity, and Z cross section. The result gives a 7% uncertainty which is applied as a systematic on conversion ID.

V. DETECTOR ACCEPTANCE AND SIGNAL RESOLUTION

The detector acceptance was studied using PYTHIA Monte Carlo production events passed through a simulation for the CDF detector, CDFSIM, based on GEANT [15] and GFLASH [16]. The remaining events that additionally passed the same photon ID selection as the data were then used to obtain an overall signal acceptance for each signal process and mass point. These values are multiplied by the z vertex efficiency, the trigger efficiency, and the data-MC correction factors to obtain acceptance times efficiency values (ϵA) for each Higgs boson test hypothesis, diphoton category, and production method (provided in Appendix A). Signal mass shapes from PYTHIA are furthermore corrected to a higher-order diphoton transverse momentum prediction from the HqT program [17–19].

VI. SYSTEMATIC UNCERTAINTIES ON SIGNAL

Systematic uncertainties on signal MC are summarized in Table II and include uncertainties in the production cross section, the integrated luminosity, and on the acceptance and efficiency. A 6% uncertainty on the integrated luminosity considers uncertainty in $p\bar{p}$ inelastic cross section and acceptance of CDF’s luminosity monitor. The theoretical uncertainties on the production cross sections used are 14% for gluon fusion, 7% for associative Higgs production with a W or Z , and 5% for vector boson fusion. All systematics on ID efficiency for photons were described in section IV.

The PDF uncertainty on event acceptance was calculated using the CTEQ61.M [20, 21] error sets and a standard event re-weighting technique [22, 23]. Initial and final state radiation (ISR and FSR) uncertainties were studied using MC samples with modified parton shower parameters. The energy scale systematic uncertainty of the central/plug electromagnetic calorimeters (CEM/PEM) was studied by checking the effect on the acceptance of varying the CEM/PEM scale by 1% to obtain 0.1% for central and 0.8% for plug. The z vertex uncertainty is based on the uncertainty in the $|z| < 60$ cm requirement described in Section III. The trigger efficiency uncertainty is based on differences in the efficiency predicted from the MC compared with that from the data.

CDF Run II Preliminary	$\int \mathcal{L} = 10.0 \text{ fb}^{-1}$			
	Systematic Errors on Signal (%)			
	CC	CP	C’C	C’P
Luminosity	6	6	6	6
$\sigma_{\text{GF}}/\sigma_{\text{VH}}/\sigma_{\text{VBF}}$	14/ 7/ 5	14/ 7/ 5	14/ 7/ 5	14/ 7/ 5
PDF	5	2	5	2
ISR/FSR	3	4	2	5
Energy Scale	0.2	0.8	0.1	0.8
Trigger Efficiency	1	1.3	1.5	6
z Vertex	0.07	0.07	0.07	0.07
Conversion ID	–	–	7	7
Material Uncertainty	0.4	3.0	0.2	3.0
Photon/Electron ID	1.0	2.8	1.0	2.6
Run Dependence	3.0	2.5	1.5	2.0
Data/MC fits	0.4	0.8	1.5	2.0

TABLE II: Summary of systematic uncertainties applied to Higgs boson signal prediction.

VII. BACKGROUND MODEL

The decay of a Higgs boson into a photon pair would appear as a very narrow peak in the invariant mass distribution of the two photons (see Figure 2). The diphoton mass resolution, as determined from simulation and checked using $Z \rightarrow e^+e^-$ decays in data, is better than $3 \text{ GeV}/c^2$ for the Higgs boson mass regions and diphoton channels studied here and is mostly limited by the energy resolution of the EM calorimeters [26].

The total background prediction is estimated from a fit made to the data using a binned log-likelihood ($\log \ell$) method. The data are fit to a sum of two exponentials multiplied by a fractional-degree polynomial, where the degree of one term is a parameter of the fit. Channels with a plug photon have a non-negligible contamination from Z boson decays and additionally include a Breit-Wigner function to model this background. The fit is performed for each m_H hypothesis in $5 \text{ GeV}/c^2$ steps from 100 to 150 GeV/c^2 . At each step a mass window centered on the Higgs boson

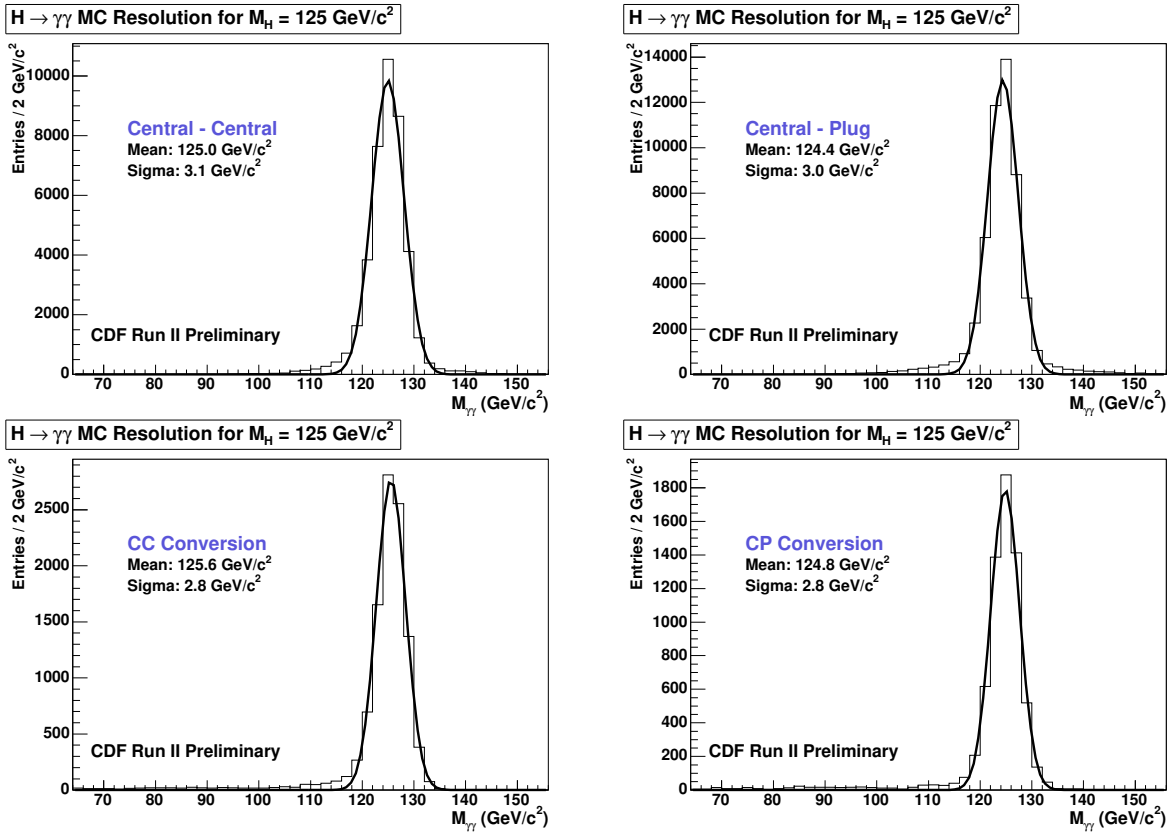


FIG. 2: Invariant mass distribution for each channel for a theoretical Higgs mass of $m_H = 125 \text{ GeV}/c^2$, showing a Gaussian width of $\sigma = 3 \text{ GeV}/c^2$ or less. A mass signal region from this resolution is selected, designed to retain approximately 95% of the signal. The shape is used when setting limits.

mass being tested is excluded. These signal mass regions are chosen to include 95% of the signal and are $12 \text{ GeV}/c^2$ for $m_H = 100\text{--}115 \text{ GeV}/c^2$, $16 \text{ GeV}/c^2$ for $m_H = 120\text{--}135 \text{ GeV}/c^2$, and $20 \text{ GeV}/c^2$ for $m_H = 140\text{--}150 \text{ GeV}/c^2$. An example fit for each channel, obtained from a mass window around $125 \text{ GeV}/c^2$, is shown in Figures 3 – 4, along with the corresponding residual plot of $(\text{data} - \text{fit})/(\text{stat error})$.

The stability of each fit in the signal region used for setting limits was studied by fluctuating the parameter values of the fit and then taking the average of the smallest and largest integral differences from that of the standard function. In general, these values reflect the statistics in the respective mass distributions as higher statistics constrains the amount by which the fit will fluctuate as parameter values are varied. The results were used to obtain a background rate uncertainty for each mass, which are on average 2.7%, 1.2%, 5.9%, and 3.2% for the CC, CP, C'C, and C'P channels, respectively.

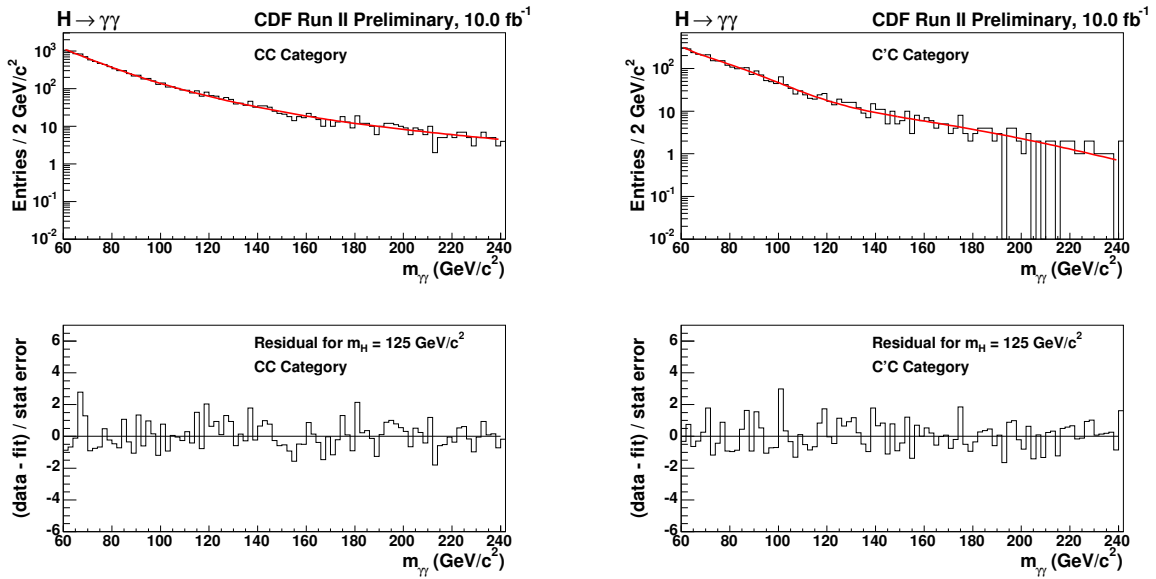


FIG. 3: Smooth fits to the signal region in the data for CC channels with the SM Higgs event selection. The example fit shown was obtained by first excluding a $16 \text{ GeV}/c^2$ window around a signal mass of $m_H = 125 \text{ GeV}/c^2$ and then interpolating into this region. The fit in the signal region will serve as the null hypothesis background model. The data-fit residual is also shown.

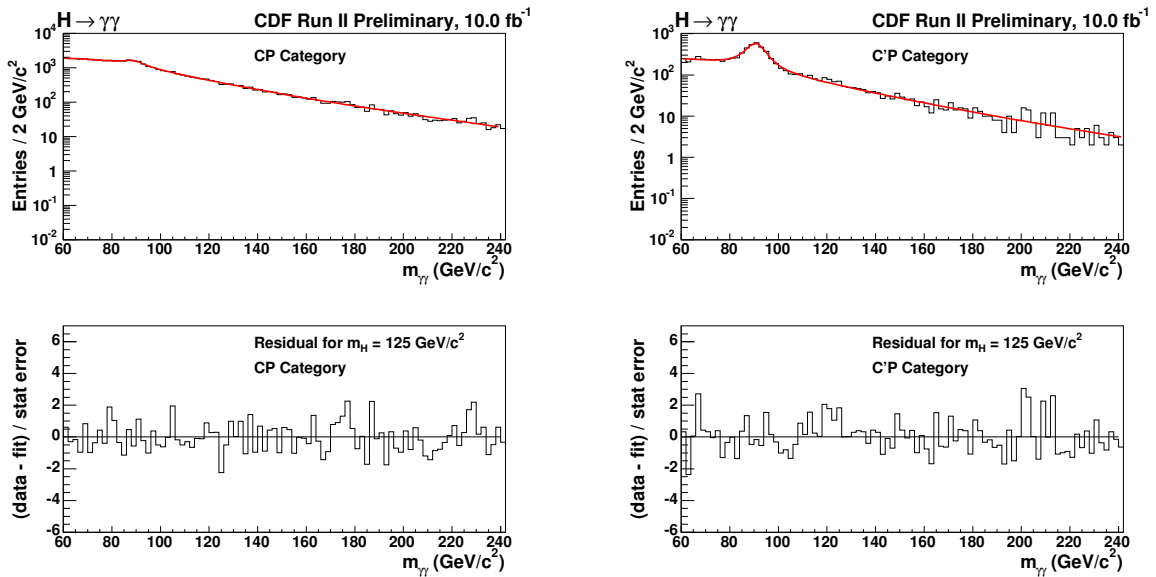


FIG. 4: A smooth fit combined with a fit function to model the $Z \rightarrow e^+e^-$ contribution for the CP channels. These example plots show fits to the signal region in the data with the SM Higgs event selection. The example fit shown was obtained by first excluding a $16 \text{ GeV}/c^2$ window around a signal mass of $m_H = 125 \text{ GeV}/c^2$ and then interpolating into this region. The fit in the signal region will serve as the null hypothesis background model. The data-fit residual is also shown.

VIII. RESULTS

No excess is observed in the data and upper limits are set on production cross sections times branching fraction. Appendix A provides the data and predicted background yields for each mass and diphoton category. The theoretical production cross section and branching fraction from Table I are used, along with the detector acceptance multiplied by efficiency, to predict the expected signal yield for each mass and channel, also shown in Appendix A. These event yields, along with the invariant mass distributions, are used to set limits on $H \rightarrow \gamma\gamma$ production.

We calculate a Bayesian C.L. limit for each Higgs boson mass hypothesis based on a combination of binned likelihoods for all channels using each bin in the signal region ($2 \text{ GeV}/c^2$ bin width) of each mass distribution. We use a flat prior in $\sigma \times B(H \rightarrow \gamma\gamma)$ and integrate over the priors for the systematic uncertainties. A 95% C.L. limit is determined such that 95% of the posterior density for $\sigma \times B(H \rightarrow \gamma\gamma)$ falls below the limit [24]. The expected 95% C.L. limits are calculated assuming no signal, based on expected backgrounds only, as the median of simulated experiments. The observed 95% C.L. on $\sigma \times B(H \rightarrow \gamma\gamma)$ are calculated from the data.

Limits calculated for each channel alone can be found in Appendix B. The combined limit results using all four channels are displayed in Table III and graphically in Fig. 5, relative to the SM theory prediction. The invariant mass distribution of the two photons for each channel with data, background, and signal shapes for an example Higgs test mass of $125 \text{ GeV}/c^2$ is shown in Figure 6.

CDF Run II Preliminary		$\int \mathcal{L} = 10.0 \text{ fb}^{-1}$				
m_H (GeV/c^2)	95% C.L. Limit/ $\sigma(\text{SM}) \times B(H \rightarrow \gamma\gamma)$					
	-2σ	-1σ	Median Exp	$+1\sigma$	$+2\sigma$	Observed
100	6.8	9.3	13.0	18.1	24.8	10.8
105	6.1	8.4	11.7	16.5	22.6	9.1
110	6.0	8.1	11.4	16.1	21.6	7.3
115	5.7	7.7	10.9	15.1	20.9	11.5
120	5.7	7.7	10.7	14.9	20.3	20.6
125	5.7	7.7	10.6	15.0	20.1	17.0
130	6.1	8.2	11.4	16.0	22.4	15.0
135	6.8	9.1	12.6	17.6	24.1	14.4
140	7.6	10.2	14.5	20.3	27.7	21.6
145	9.2	12.5	17.6	25.0	34.3	18.5
150	12.4	16.7	23.1	32.6	44.6	13.1

TABLE III: 95% upper confidence level limits on cross sections times branching ratio relative to SM prediction for all channels combined.

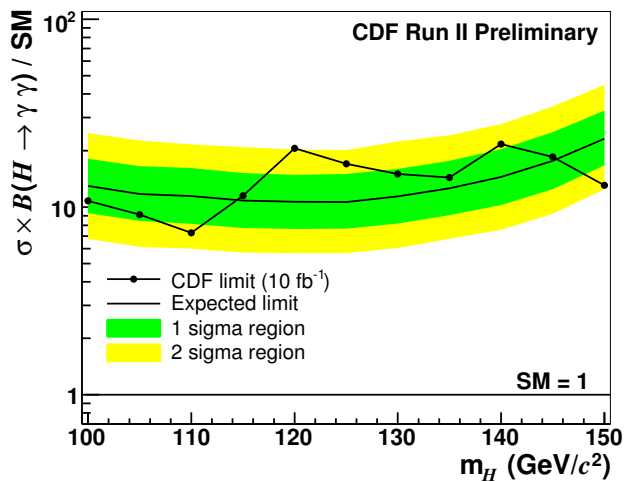


FIG. 5: 95% upper confidence level limits on cross sections times branching fraction relative to SM prediction for all channels combined.

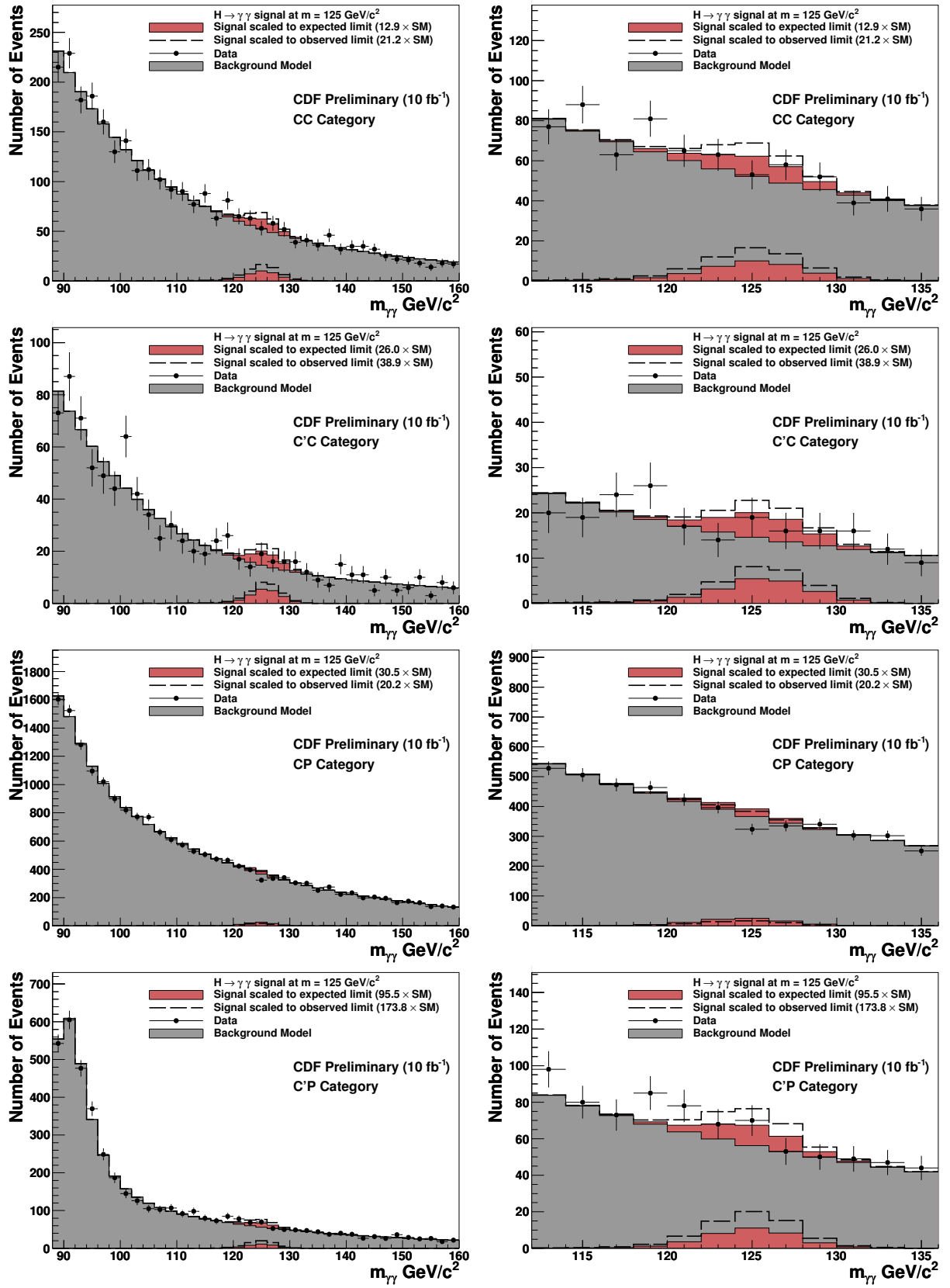


FIG. 6: Invariant mass distribution over whole mass range and zoomed in, with an example theoretical Higgs mass at $125 \text{ GeV}/c^2$, scaled to the expected and observed limits obtained from the respective channel alone.

IX. CONCLUSIONS

An analysis was discussed which searched for a $H \rightarrow \gamma\gamma$ resonance in the diphoton mass spectrum using 10 fb^{-1} and the inclusion of central, forward, and central conversion photons. This analysis improves upon the previous 7.0 fb^{-1} result with the incorporation of approximately 43% more data. No significant excess over the background was observed, so we presented 95% C.L. upper limits on the production cross sections times branching fraction relative to the SM expectation. For Higgs masses between 100 and 150 GeV the expected limits range from 10.6 to 23.1 and observed limits range from 7.3 to 21.6. This is an approximate 20% improvement in sensitivity compared to the previous CDF result [4].

Acknowledgments

We thank the Fermilab staff and the technical staffs of the participating institutions for their vital contributions. This work was supported by the U.S. Department of Energy and National Science Foundation; the Italian Istituto Nazionale di Fisica Nucleare; the Ministry of Education, Culture, Sports, Science and Technology of Japan; the Natural Sciences and Engineering Research Council of Canada; the National Science Council of the Republic of China; the Swiss National Science Foundation; the A.P. Sloan Foundation; the Bundesministerium fuer Bildung und Forschung, Germany; the Korean Science and Engineering Foundation and the Korean Research Foundation; the Particle Physics and Astronomy Research Council and the Royal Society, UK; the Russian Foundation for Basic Research; the Comision Interministerial de Ciencia y Tecnologia, Spain; and in part by the European Community's Human Potential Programme under contract HPRN-CT-20002, and the Academy of Finland.

-
- [1] ATLAS Collaboration (2012), ATLAS-CONF-2012-091.
 - [2] CMS Collaboration (2012), CMS-PAS-HIG-12-015.
 - [3] V. Abazov et al. (D0 Collaboration), Phys. Rev. Lett. **107**, 151801 (2011).
 - [4] T. Aaltonen et al. (CDF Collaboration), Phys. Rev. Lett. **108**, 011801 (2012).
 - [5] S. Mrenna and J. D. Wells, Phys. Rev. **D63**, 015006 (2001), hep-ph/0001226.
 - [6] CDF Collaboration (2011), CDF note 10731.
 - [7] M. Spira (1998), hep-ph/9810289.
 - [8] F. Abe et al. (CDF), Nucl. Instr. Meth. **A271**, 387 (1988).
 - [9] P. T. Lukens (CDF IIB) (2003), FERMILAB-TM-2198.
 - [10] T. Sjostrand et al., Comput. Phys. Commun. **135**, 238 (2001), hep-ph/0010017.
 - [11] H. L. Lai et al. (CTEQ), Eur. Phys. J. **C12**, 375 (2000), hep-ph/9903282.
 - [12] R. Field and R. C. Group (CDF) (2005), hep-ph/0510198.
 - [13] T. Aaltonen et al. (CDF Collaboration), Phys. Rev. D **82**, 052005 (2010).
 - [14] F. Abe et al. (CDF Collaboration), Phys. Rev. D **48**, 2998 (1993).
 - [15] R. Brun, F. Bruyant, M. Maire, A. C. McPherson, and P. Zancarini (1987), CERN-DD/EE/84-1.
 - [16] G. Grindhammer, M. Rudowicz, and S. Peters, Nucl. Instrum. Meth. **A290**, 469 (1990).
 - [17] G. Bozzi, S. Catani, D. de Florian, and M. Grazzini, Phys. Lett. B **564**, 65 (2003), hep-ph/0302104.
 - [18] G. Bozzi, S. Catani, D. de Florian, and M. Grazzini, Nucl. Phys. B **737**, 73 (2006), hep-ph/0508068.
 - [19] D. de Florian, G. Ferrera, M. Grazzini, and D. Tommasini, JHEP **1111**, 064 (2011), 1109.2109.
 - [20] D. Stump et al., JHEP **10**, 046 (2003), hep-ph/0303013.
 - [21] J. Pumplin et al., Phys. Rev. **D65**, 014013 (2002), hep-ph/0101032.
 - [22] P. M. Nadolsky and Z. Sullivan, eConf **C010630**, P510 (2001), hep-ph/0110378.
 - [23] D. Bourilkov, R. C. Group, and M. R. Whalley (2006), hep-ph/0605240.
 - [24] K. Nakamura et al. (Particle Data Group), Phys. Lett. G **37**, 075021 (2010).
 - [25] The transverse energy E_T and transverse momentum p_T are defined as $E \sin \theta$ and $|\vec{p}| \sin \theta$, respectively.
 - [26] The natural width of the Higgs boson is negligible. The mass resolution is also sensitive to the selection of the correct primary vertex of the $p\bar{p}$ interaction. This effect is studied using Z decays in the data and found to be well modeled in the simulation.

Appendix A: Event Yields and Signal Acceptances

TABLE IV: For each SM Higgs boson mass hypotheses tested in this analysis, the efficiency multiplied by signal acceptance (ϵA) is shown as a percentage of the total number of $H \rightarrow \gamma\gamma$ decays for each production mechanism (GF, VH, and VBF). These values, along with the cross sections and branching ratios provided in Table I, are used to obtain the predicted number of SM Higgs boson signal events. Integrated luminosities for each channel are given in Section III and provided in each subtable. The number of background and data events are also given for each mass. The final column in each subtable is the number of signal events divided by the square root of the number of background events (S/\sqrt{B}). The event yields for each mass point are obtained from a signal region centered on the Higgs boson mass hypothesis, allowing slight overlap between signal regions.

(a)								(b)									
SM $H \rightarrow \gamma\gamma$				CDF Run II Preliminary				SM $H \rightarrow \gamma\gamma$				CDF Run II Preliminary					
CC Category (10 fb^{-1})								CP Category (9.3 fb^{-1})									
m_H (GeV/ c^2)	ϵA (%)			Event Yields				S/\sqrt{B}	m_H (GeV/ c^2)	ϵA (%)			Event Yields				S/\sqrt{B}
	GF	VH	VBF	Signal	Background	Data	GF			VH	VBF	Signal	Background	Data			
100	9.9	10.2	11.1	3.8	857	840	0.13	100	11.5	10.3	10.3	3.9	5427	5378	0.05		
105	10.0	10.2	11.1	3.7	725	688	0.14	105	11.7	10.4	10.6	3.9	4524	4535	0.06		
110	10.0	10.3	11.2	3.6	566	561	0.15	110	11.9	10.6	10.8	3.8	3636	3651	0.06		
115	10.0	10.3	11.2	3.4	479	491	0.16	115	11.9	10.7	10.9	3.6	3179	3155	0.06		
120	10.6	10.7	11.6	3.3	507	548	0.15	120	12.5	11.3	11.5	3.6	3520	3450	0.06		
125	10.6	10.8	11.6	3.0	440	474	0.14	125	12.4	11.3	11.5	3.2	3067	3061	0.06		
130	10.7	10.9	11.8	2.6	362	388	0.14	130	12.4	11.3	11.6	2.8	2536	2529	0.06		
135	10.8	10.9	11.7	2.2	323	339	0.13	135	12.4	11.4	11.6	2.3	2224	2265	0.05		
140	11.1	11.3	12.1	1.9	337	343	0.10	140	12.7	11.7	11.9	1.9	2342	2351	0.04		
145	11.3	11.3	12.1	1.5	300	302	0.09	145	12.7	11.7	11.8	1.5	2071	2084	0.03		
150	11.2	11.3	12.2	1.1	265	237	0.07	150	12.6	11.7	11.8	1.1	1749	1746	0.03		

(c)								(d)									
SM $H \rightarrow \gamma\gamma$				CDF Run II Preliminary				SM $H \rightarrow \gamma\gamma$				CDF Run II Preliminary					
C'C Category (9.9 fb^{-1})								C'P Category (9.3 fb^{-1})									
m_H (GeV/ c^2)	ϵA (%)			Event Yields				S/\sqrt{B}	m_H (GeV/ c^2)	ϵA (%)			Event Yields				S/\sqrt{B}
	GF	VH	VBF	Signal	Background	Data	GF			VH	VBF	Signal	Background	Data			
100	2.6	2.6	2.8	1.0	287.0	285	0.03	100	1.4	1.2	1.2	0.5	1170	1182	0.01		
105	2.6	2.5	2.8	0.9	232.6	239	0.04	105	1.5	1.3	1.4	0.5	841	773	0.02		
110	2.7	2.6	2.9	0.9	194.2	152	0.04	110	1.5	1.3	1.3	0.5	598	585	0.02		
115	2.7	2.5	2.8	0.9	151.4	143	0.04	115	1.5	1.3	1.4	0.5	500	535	0.02		
120	2.9	2.8	3.0	0.9	155.4	155	0.04	120	1.6	1.4	1.4	0.5	526	605	0.02		
125	2.9	2.7	3.0	0.8	124.5	148	0.04	125	1.6	1.4	1.4	0.4	470	526	0.02		
130	2.9	2.7	3.0	0.7	106.5	109	0.04	130	1.7	1.4	1.5	0.4	409	418	0.02		
135	2.8	2.7	3.0	0.6	91.4	102	0.03	135	1.6	1.4	1.5	0.3	365	357	0.02		
140	2.9	2.8	3.0	0.5	99.1	101	0.03	140	1.7	1.4	1.5	0.3	388	374	0.01		
145	2.9	2.8	3.0	0.4	88.0	89	0.02	145	1.7	1.5	1.5	0.2	346	332	0.01		
150	3.0	2.8	3.1	0.3	78.1	75	0.02	150	1.7	1.5	1.5	0.1	290	277	0.01		

Appendix B: Limits Per Channel

TABLE V: Expected and observed limits on production cross section multiplied by $H \rightarrow \gamma\gamma$ branching ratio relative to the SM prediction, calculated for each diphoton category alone.

(a)							(b)						
CC Category		CDF Run II Preliminary, 10 fb ⁻¹					CP Category		CDF Run II Preliminary, 10 fb ⁻¹				
m_H (GeV/c ²)	95% C.L. Limit/ $\sigma(\text{SM}) \times B(H \rightarrow \gamma\gamma)$						m_H (GeV/c ²)	95% C.L. Limit/ $\sigma(\text{SM}) \times B(H \rightarrow \gamma\gamma)$					
	-2 σ	-1 σ	Median Exp	+1 σ	+2 σ	Observed		-2 σ	-1 σ	Median Exp	+1 σ	+2 σ	Observed
100	8.1	10.8	15.1	21.3	29.5	11.3	100	21.3	29.0	40.8	57.2	76.8	30.0
105	7.5	9.9	14.1	19.9	27.7	10.6	105	18.6	25.4	35.3	49.3	68.8	54.1
110	7.1	9.7	13.5	19.1	26.5	11.4	110	17.5	23.6	32.7	45.2	62.1	26.8
115	6.8	9.1	12.9	18.2	25.2	15.4	115	16.5	22.1	31.0	43.8	58.8	26.9
120	6.7	9.2	12.8	18.2	25.1	22.2	120	16.7	22.4	30.8	43.7	60.0	36.7
125	6.8	9.3	12.9	18.2	24.7	21.2	125	16.3	22.0	30.5	43.0	58.1	20.2
130	7.3	10.0	13.9	19.6	26.6	16.0	130	17.3	23.4	32.8	45.7	62.6	36.1
135	7.9	10.8	15.3	21.2	29.3	17.2	135	19.1	25.4	36.0	50.8	68.7	44.4
140	9.3	12.6	17.5	24.8	33.7	25.4	140	21.5	29.7	41.7	58.7	79.0	43.2
145	11.2	15.2	21.2	29.8	41.3	24.3	145	26.3	35.5	49.9	70.1	96.9	52.8
150	14.8	20.5	28.2	40.0	55.7	15.1	150	34.5	45.6	64.8	90.4	126.4	65.5

(c)							(d)						
C'C Category		CDF Run II Preliminary, 10 fb ⁻¹					C'P Category		CDF Run II Preliminary, 10 fb ⁻¹				
m_H (GeV/c ²)	95% C.L. Limit/ $\sigma(\text{SM}) \times B(H \rightarrow \gamma\gamma)$						m_H (GeV/c ²)	95% C.L. Limit/ $\sigma(\text{SM}) \times B(H \rightarrow \gamma\gamma)$					
	-2 σ	-1 σ	Median Exp	+1 σ	+2 σ	Observed		-2 σ	-1 σ	Median Exp	+1 σ	+2 σ	Observed
100	18.7	25.5	36.2	51.3	70.9	58.6	100	75.2	102.9	144.4	204.7	285.0	100.8
105	16.8	22.8	31.9	44.5	60.9	23.8	105	63.3	85.7	121.3	171.9	241.0	62.7
110	16.5	22.3	31.1	43.8	60.9	16.2	110	56.6	77.2	108.4	153.7	212.3	121.5
115	14.7	20.0	28.3	40.2	56.5	24.7	115	54.4	72.4	101.6	144.4	199.3	129.7
120	13.9	18.9	26.6	37.9	52.2	31.3	120	47.5	65.6	91.9	131.1	181.7	215.0
125	13.7	18.7	26.0	37.1	50.5	38.9	125	49.1	68.2	95.5	134.9	188.9	173.8
130	15.2	20.4	28.7	40.3	57.2	39.3	130	54.6	73.7	103.1	145.4	202.8	98.7
135	16.9	22.8	32.0	45.1	62.7	30.8	135	60.6	82.4	114.8	165.6	225.8	106.4
140	19.5	26.7	37.2	54.1	74.8	49.5	140	71.2	96.2	134.7	190.6	259.0	106.2
145	24.8	33.2	46.9	67.3	94.8	43.4	145	84.8	113.4	159.1	227.9	311.6	112.0
150	32.0	43.5	60.7	86.5	118.7	50.4	150	110.0	151.8	212.5	297.5	413.5	246.1

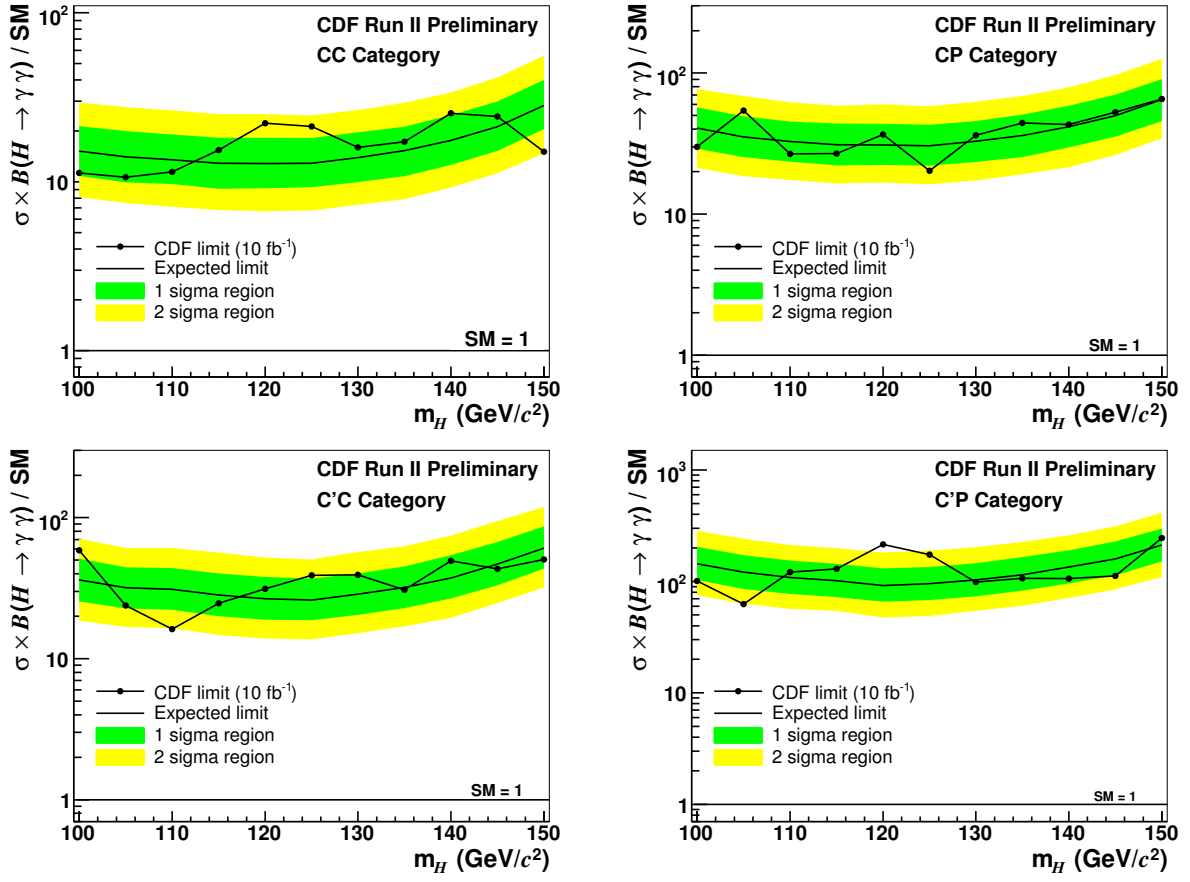


FIG. 7: Expected and observed limits on production cross section multiplied by $H \rightarrow \gamma\gamma$ branching fraction relative to the SM prediction, calculated for each diphoton category alone.